Available online at www.sciencedirect.com

jmr&t
Journal of Materials Research and Technology
www.jmrt.com.br

Original article

Studies of the anticorrosion property of a newly synthesized Green isoxazolidine for API 5L X60 steel in acid environment

Mouheddin T. Alhaffar[a], *Saviour A. Umoren*[b,*], *Ime B. Obot*[b], *Shaikh A. Ali*[a], *Moses M. Solomon*[b]

[a] *Department of Chemistry, Faculty of Science, King Fahd University of Petroleum and Minerals, Dhahran 31261, Saudi Arabia*
[b] *Centre for Research Excellence in Corrosion, Research Institute, King Fahd University of Petroleum and Minerals, Dhahran 31261, Saudi Arabia*

ARTICLE INFO

Article history:
Received 1 November 2018
Accepted 24 July 2019
Available online 14 August 2019

Keywords:
Isoxazolidine compounds
Theoretical studies
Corrosion inhibitor
Acid corrosion
Steel

ABSTRACT

The potential of an environmentally friendly novel synthesized and characterized isoxazolidine derivative namely 5-(4-dodecyloxy-3-methoxybenzyl)-2-methylisoxazolidine (DMBMI) as anticorrosion agent for carbon steel in 1 mol/L HCl solution was investigated using gravimetric and electrochemical techniques. Kinetics parameters of the corrosion process and the thermodynamic data of adsorption of the organic molecule on the carbon steel surface was also assessed in order to characterize the performance of the studied compound as a corrosion inhibitor. The solubility, toxicity and the state of the molecule at the acidic pH (1 mol/L HCl) was predicted. It was found that the synthesized compound is green (environmentally friendly) with an optimum solubility of 23.8 mg/L. Also the molecule exists 100 percent in protonated form in 1 mol/L HCl (pH = 0). The molecule possesses anticorrosion property against steel corrosion in acid environment. Corrosion retardation efficacy is dependent on concentration and temperature. DMBMI exhibited concentration dependent corrosion inhibition ability influencing mainly anodic metal dissolution based on potentiodynamic polarization data. Addition of KI through the mechanism of competitive adsorption enhanced the inhibition efficiency considerably. The active sites for the interaction of DMBMI with steel surface was calculated using quantum chemical method while the adsorption energy between the inhibitor and steel surface was derived via Monte Carlo simulations. Results from theoretical studies and surface analysis are in conformity and reveal that the O and N heteroatoms in the synthesized molecule are the interaction centers.

1. Introduction

Mineral acid solutions are widely deployed in many industrial processes. One of such processes is acid pickling, a process of getting rid of surface impurities from ferrous and non-ferrous metals. Since acid solution is corrosive, it is customary

* *Corresponding author.*
E-mail: umoren@kfupm.edu.sa (S.A. Umoren).
https://doi.org/10.1016/j.jmrt.2019.07.051

Table 1 – Requirements for corrosion inhibitors developed in the present time.

- Biodegradation > 70% in 28 days
- Excellent solubility
- Bioaccumulation log $P_o/w < 3$
- Toxicity > 10 mg/L (LD_{50} or LC_{50})

Criteria to estimate toxicity (LD_{50} or LC_{50})

Criteria	Category				
	1	2	3	4	5
Oral (mg/kg)	5	50	300	2000	**5000**
Dermal (mg/kg)	50	200	1000	2000	
Gases (mg/L/4h)	100	500	2500	20000	
Vapors (mg/l/4h)	0.5	2	10	20	
Dust & Mists (mg/l/4h)	0.05	0.5	1	5	

Summary of category

Category 1	Category 2	Category 3	Category 4	Category 5
 Fatal if swallowed	 Fatal if swallowed	 Fatal if swallowed	 Harmful if swallowed	NO SYMBOL May be Harmful if swallowed

- *A green inhibitor is expected to belong to category 4 or 5.*

to fortify the solution with corrosion inhibitors to control metallic structures corrosion. Corrosion inhibitors are inorganic or organic molecules that are added in part per million (ppm) levels to form surface layers that decrease the corrosion rate of metals. Diverse inhibitors are used depending on the actual conditions of the corrosive environment as well as the metallurgy. New corrosion inhibitors are constantly being developed to tackle corrosion problems in various aggressive environments [1–3]. Ultimately, a new chemical must be green compliant. Greenness is defined based on four criteria: solubility, biodegradation, bioaccumulation, and toxicity [4,5]. A new chemical developed in the present time should possess excellent solubility, have log P_o/w value of less than 3, LD_{50}/LC_{50} value that falls within category of 4 or 5, and 70% of it should degrade within 28 days [4–6]. In Table 1 is presented the criteria for the classification of corrosion inhibitor as green.

Isoxazolidine is a five-membered heterocyclic compound containing adjacent nitrogen and oxygen atoms. For decades, it has been utilized in the manufacturing of green products for biological applications [7,8]. It is an essential scaffold in drug discovery where it mimics a wide range of natural building blocks [8]. Derivatives of isoxazolidine have been assessed for anticorrosion property for steel in HCl [9–11], H_2SO_4 [12,13], CO_2 [14], and saline [14] media. In these corrosive environments, depending on experimental conditions (pH, concentration of inhibitor, temperature), length of hydrophobic chain of the isoxazolidine derivative, and the degree of steric crowding around the nitrogen centers, inhibition efficiency in the range of 40–99% was obtained.

Blending of two or more substances to enhance inhibition efficiency is a common modification approach. Metals ions like zinc ions [15,16] and halide ions particularly iodide ions [17,18] have been established to boost the anticorrosion property of organic inhibitors when added. A detailed information on the effect of addition of metals and halides ions on organic inhibitors can be found in Umoren and Solomon [19,20]. In this communication, we present 5-(4-dodecyloxy-3-methoxybenzyl)-2-methylisoxazolidine (Fig. 1) (DMBMI)/iodide ions formulation as a novel, cheap, green, and effective corrosion inhibitor that can be utilized during the pickling of low carbon steel. The characterization of DMBMI was done spectroscopically via nuclear magnetic resonance (NMR) and Fourier-transform infrared (FTIR) spectroscopies. The evaluation of DMBMI as corrosion inhibitor was performed using weight loss, electrochemical impedance spectroscopy, potentiodynamic polarization, and linear polarization techniques. The adsorption of DMBMI molecules on sample surfaces was verified via SEM (scanning electron microscope), FTIR, and EDAX (energy dispersive X-ray spectroscopy).

The use of the computational chemistry techniques to evaluate inhibitor-metal interactions is becoming popular

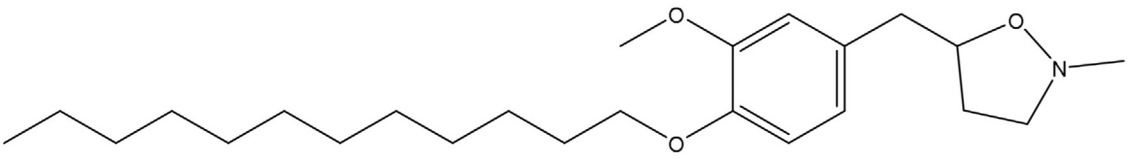

5-(4-dodecyloxy-3-methoxybenzyl)-2-methylisoxazolidine

Fig. 1 – Molecular structure of 5-(4-dodecyloxy-3-methoxybenzyl)-2-methylisoxazolidine.

[21–23]. This is because the theoretical techniques have the capacity to predict important chemical parameters that could help researchers in discovering promising inhibitor molecules [24,25]. It can as well provide insight into the mechanism of interaction between inhibitor molecules and a metal surface [23]. In this work, we used the molecular modeling (quantum chemical calculations and Monte Carlo simulation) approaches to predict the active sites and the adsorption property of DMBMI. For the first time, with the help of ACD/Percepta™ -14 Software (ACD/Labs, Toronto, Canada) Licensed to King Fahd University of Petroleum and Minerals, 2017, we have predicted accurately the solubility, toxicity, and the exact state of DMBMI in 1 mol/dm^3 HCl solution.

2. Experimental

2.1. Materials

N-Methylhydroxylamine hydrochloride (98%), 1-bromododecane (97%), Silica gel 100, paraformaldehyde (Fluka Chemie AG) (95%), and eugenol (1) (99%) were purchased from Aldrich Co.

2.2. Physical methods

The elemental analyses and the recording of the FTIR spectra were accomplished by utilizing a Perkin Elmer Series II Model 2400 and a Perkin Elmer (16 F PC) spectrometer respectively. The nuclear magnetic resonance (NMR) spectra were obtained in D_2O on a 500-MHz JEOL LA spectrometer; the residual proton resonance of D_2O at δ 4.65 mg/L and the dioxane ^{13}C peak at δ 67.4 mg/L were taken as an internal and external standard, respectively.

2.3. Synthesis

2.3.1. -Allyl-1-dodecyloxy-2-methoxybenzene (2)

To a solution of NaOH (4.8 g, 0.12 mol) in ethanol (60 mL) was added eugenol (1) (19.7 g, 0.12 mol) followed by 1-bromododedcane (24.9 g, 0.10 mol) and the mixture was heated at 60 °C under N_2 for 24 h. After removal of the solvent, the mixture was taken up in ether (75 mL) and washed with 10% NaOH (2 × 50 mL) and water (2 × 50 mL). The organic layer was dried (Na_2SO_4) and concentrated to obtain alkene 2 as a white solid (31.7 g, 95%). MP 28–29 °C; (Found: C, 79.2; H, 10.7. $C_{22}H_{36}O_2$ requires C, 79.46; H, 10.91%); $\nu_{max.}$ (KBr) 3079, 3053, 2999, 2919, 2849, 1638, 1608, 1589, 1518, 1468, 1418, 1395, 1376, 1339, 1299, 1286, 1232, 1188, 1160, 1138, 1062, 1035, 999, 964, 914, 850, 797, 768, 751, 720, 650, 607, and 592 cm^{-1}; δ_H ($CDCl_3$) 0.88 (3H, t, *J* 7.0 Hz), 1.26 (16H, m), 1.44 (2H, m), 1.82 (2H, quint, *J* 7.3 Hz), 3.32 (2H, d, *J* 6.4 Hz), 3.84 (3H, s), 3.98 (2H, t, *J* 7.0 Hz), 5.06 (2H, m), 5.95 (1H, m), 6.69 (1H, d, *J* 8.0 Hz), 6.72 (1H, s), 6.80 (1H, d, *J* 8.0 Hz); δ_C ($CDCl_3$) 14.08, 22.66, 25.94, 29.20, 29.32, 29.39, 29.54, 29.57, 29.61, 29.62, 31.89, 39.78, 55.90, 69.15, 112.32, 113.09, 115.50, 120.40, 132.57, 137.70, 146.91, 149.33.

2.3.2. 5-(4-Dodecyloxy-3-methoxybenzyl)-2-methylisoxazolidine (5)

A mixture *N*-methylhydroxylamine hydrochloride (**3**) (3.34 g, 40.0 mmol), sodium acetate trihydrate (5.85 g, 43 mmol), paraformaldehyde (1.80 g, 60 mmol) and alkene **2** (16.6 g, 50 mmol) in ethanol (35 cm^3) was strirred using a magnetic stir bar at 110 °C in a closed pressure vessel for 7 h. After removal of solvent, the mixture was basified (K_2CO_3 solution (50 mL)) and extracted with ether (2 × 50 cm^3). The organic layer was dried (Na_2SO_4) and chromatographed over silica gel using 3:1 hexane/ether as eluant to give adduct **5** as a white solid (12.9 g, 82%). Mp 39–40 °C. The synthesis route is as shown in Scheme 1. (Found: C, 73.4; H, 10.3; N, 3.5. $C_{24}H_{41}NO_3$ requires C, 73.61; H, 10.55; N, 3.58%); $\nu_{max.}$ (KBr) 2917, 2850, 1589, 1512, 1466, 1425, 1388, 1332, 1232, 1144, 1132, 1030, 944, 917, 850, 797, 727, 672, 616, 556 cm^{-1}; δ_H ($CDCl_3$): 0.88 (3H, t, *J* 7.0 Hz), 1.25–1.43 (18, m), 1.87 (2H, m), 1.92–2.02 (1H, m), 2.26–2.74 (6H, m), 2.91–2.96 (1H, m), 3.22–3.27 (1H, m), 3.88–4.00 (5H, m), 4.27 (0.5H, m), 4.45 (0.5H, m), 6.78–6.82 (3H, m); δ_C ($CDCl_3$): 14.3, 22.7, 25.9, 28.9, 29.4, 29.4, 29.6, 29.6, 29.7, 29.7, 31.9, 33.3 (0.5C), 33.7 (0.5C), 40.2 (0.5), 41.0 (0.5C), 45.1 (0.5C), 45.5 (0.5C), 55.7, 56.3 (0.5C), 57.1 (0.5C), 68.4, 78.6, 111.4 (0.5C), 111.5 (0.5C), 111.9, 120.8 (0.5C), 120.9 (0.5C), 129.8 (0.5C), 130.3 (0.5C), 146.5, 148.0 ($CDCl_3$ middle carbon: 77.4).

2.4. Studies of inhibitive property

2.4.1. Samples/corrodent preparation

Steel grade API 5 L X60 of chemical composition given in our previous publication [26] was utilized as the metal substrate in this study. Samples were made from the steel pipe and were of two categories: 3 cm × 3 cm × 1 cm for gravimetric experiments and 1 cm × 1 cm × 1 cm for electrochemical experiments. Before used, the specimens were mechanically abraded with silicon carbide papers (#120–#800 grit), sonicated in CH_3CH_2OH bath for ten minutes, degreased with CH_3CH_2OH and CH_3COCH_3, and dried in warm air [26]. The specimens for electrochemical measurements were completely insulated with Teflon tape exposing one side of surface area 1 cm^2. The prepared specimens were stored in a desiccator. The simulated corrosive environment was a molar solution of hydrochloric acid. The concentration

ranges of the synthesized compound, 5-(4-dodecyloxy-3-methoxybenzyl)-2-methylisoxazolidine (DMBMI) utilized was 20–100 mg/L while that of KI was 0.005 mol/L. Measurements were performed at temperature range of 25–60 °C.

2.4.2. *Gravimetric measurements*

The ASTM standard procedure [27] was adopted in gravimetric experiments. The prepared specimens were weighed and thereafter freely suspended in glass vessels containing test solutions (blank, 20, 40, 60, 80, & 100 mg/L DMBMI inhibited). The reaction vessels were placed in a thermostated water bath maintained at 25–60 °C for 24 h. After which, the corroded specimens were removed, immersed in a molar solution of HCl for twenty seconds to detach the corrosion products, washed with distilled water, cleansed in acetone, dried with specimen dryer, and finally reweighed to determine the loss in weight. The weight losses obtained were used to compute the corrosion rate (v) following the equation given elsewhere [26]. The equation used for the calculation of inhibition efficiency (η) can also be found in Ref. [26].

2.4.3. *Electrochemical measurements*

Electrochemical measurement was performed using Gamry Potentiostat/galvanost/ZRA (Ref 600) instrument with a conventional three-electrode assembly in a 250 mL glass cell. API 5 L X60 steel specimen embedded in thermoplastic resin with an uncovered area of 1 cm^2, graphite rod and silver/silver chloride (Ag/AgCl) were used as working, counter and reference electrodes respectively. Measurements were carried out after the working electrode was immersed for 3600 s in the various test solutions at ordinary temperature for the purpose of attaining a steady-state open-circuit potential (OCP). Frequency in the range of 100 kHz to 0.01 Hz was used for electrochemical impedance measurements and the amplitude was 10 mV peak to peak. The potentiodynamic polarization curves were recorded at a scan rate of 0.5 mV s^{-1} relative to free corrosion potential (E_{corr}) from cathodic potential of −250 mV to anodic potential of +250 mV. By extrapolation of the linear Tafel regions of the polarization curves, the corrosion current densities (i_{corr}) and other associated electrochemical parameters were obtained. Linear polarization resistance (LPR) measurements were performed by polarizing the working electrode from −15 to +15 mV versus OCP at a sweep rate of 0.125 mV/s. The polarization resistance (R_p) was obtained from the slope of the potential-current curve in the vicinity of corrosion potential (E_{corr}). We had defined the equations for the computation of inhibition efficiency from electrochemical impedance spectroscopy (EIS), potentiodynamic polarization (PDP) and LPR in our recent publication [26].

2.5. *Computational details*

2.5.1. *Solubility, protonation and toxicity prediction*

The solubility, protonation and toxicity of DMBMI were predicted using ACD/Percepta™-14 Software (ACD/Labs, Toronto, Canada) Licensed to KFUPM, 2017.

2.5.2. *Quantum chemical calculations*

Quantum Chemical based computations were conducted by the DMol^3 module implemented in the BOVIA Materials Studio (Version 8.0) from Accelyrs Inc. (San Diego, CA, USA). Geometrical optimization of DMBMI-H^+ was performed by the meta- generalized gradient approximation (m-GGA) with Minnesota 2006 local functional (M06-L) in conjunction with double numerical plus polarization (DNP) basis set. The computations were done in aqueous phase to simulate the effect of solvent. The HOMO (highest occupied molecular orbitals) and LUMO (lowest unoccupied molecular orbitals) which discloses the active sites of the molecules were plotted.

2.5.3. *Monte Carlo simulations*

The interaction between the investigated inhibitor and Fe (110) plane surface was carried out using Monte Carlo simulations. The adsorption locator code implemented in the Material Studio 8.0 software from Biovia–Accelrys Inc. USA was adopted in this simulation. The COMPASS force field was deployed for the simulation of all molecules and systems. The simulation of the corrosion inhibitor molecule (DMBMI-H^+) on Fe (110) surface was essential so as to pinpoint on the low energy adsorption sites of the potential corrosion inhibitor on Fe surface. Fifty (50) molecules of water were included in the simulation box to mimic the aqueous phase. Details of the methodology of Monte Carlo simulations are available in our previous publications [28,29].

3. Results and discussion

3.1. *Physical parameters prediction*

Three important parameters namely, solubility, protonation, and toxicity were predicted for DMBMI in 1 mol/L HCl (pH = 0) using ACD/Percepta™-14 Software. The results obtained for solubility and protonation are shown in Figs. 2 and 3, respectively. The synthesized compound (DMBMI) is soluble in 1 mol/L HCl having optimum solubility of 23.8 mg/L (Fig. 2). It is deduced from Fig. 3(a) that, in 1 mol/L HCl, 100% of DMBMI molecules exist in protonated form and the protonation is on the nitrogen heteroatoms (Fig. 3(b)). The prediction for toxicity was as follows: 90% probability that LD_{50} is less than 5000 mg/kg (category 5), 80% probability that LD_{50} is greater than 300 mg/kg (category 4), and 80% probability that the LD_{50} value of DMBMI falls within these two categories. A chemical with LD_{50} value under category 4 and 5 is adjudged green (Table 1). Since at pH = 0 (1 mol/L HCl), 100% protonated form of DMBMI is present in aqueous solution, this form was adopted for all the molecular modelings.

3.2. *Quantum chemical calculations*

Information regarding which functional group(s) in an organic molecule would participate in the process of donating and/or accepting electrons during interaction with a metal surface can be derived from HOMO and LUMO orbitals. The region in an organic molecule with large HOMO orbitals can easily give electron to free d-orbital of a metal atom [26]. Similarly, the region in organic molecule with large LUMO orbitals accept electrons from d-orbital of a metal with ease [26]. To gain insight into the regions in DMBMI facilitating interaction on the substrate surface in the considered aggressive medium,

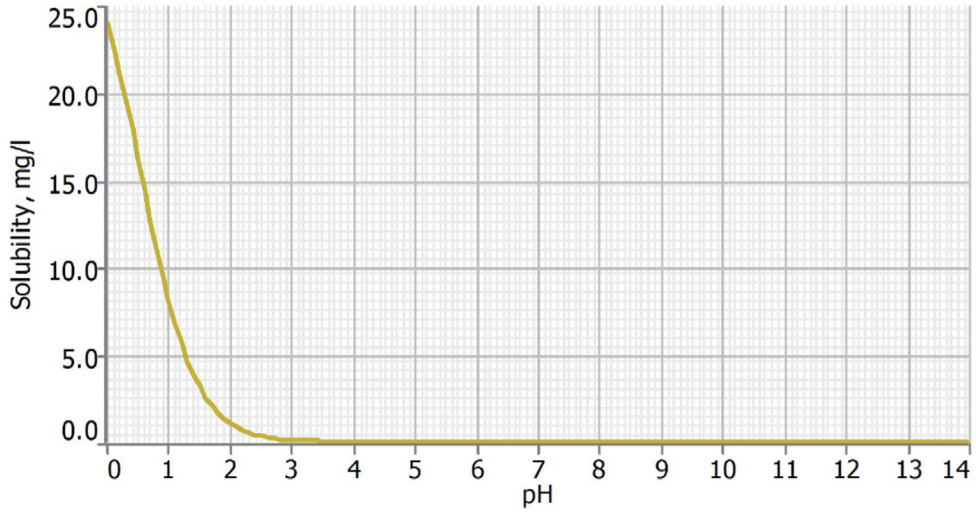

Fig. 2 – The solubility versus pH of 5-(4-dodecyloxy-3-methoxybenzyl)-2-methylisoxazolidine predicted using ACD/LABS Software.

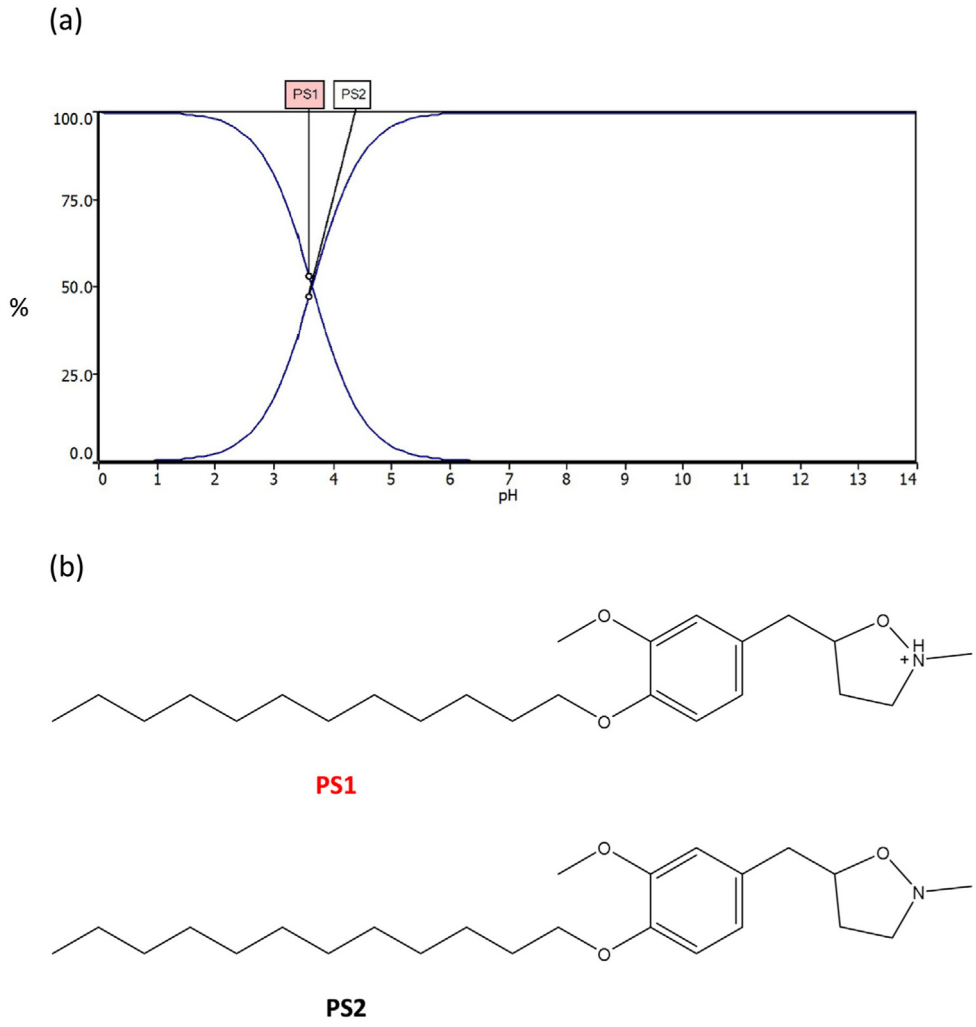

Fig. 3 – (a) The curve of protonated state vs pH of 5-(4-dodecyloxy-3-methoxybenzyl)-2-methylisoxazolidine predicted using ACD/LABS Software and (b) The molecular structures corresponding to the two states PS1 and PS2.

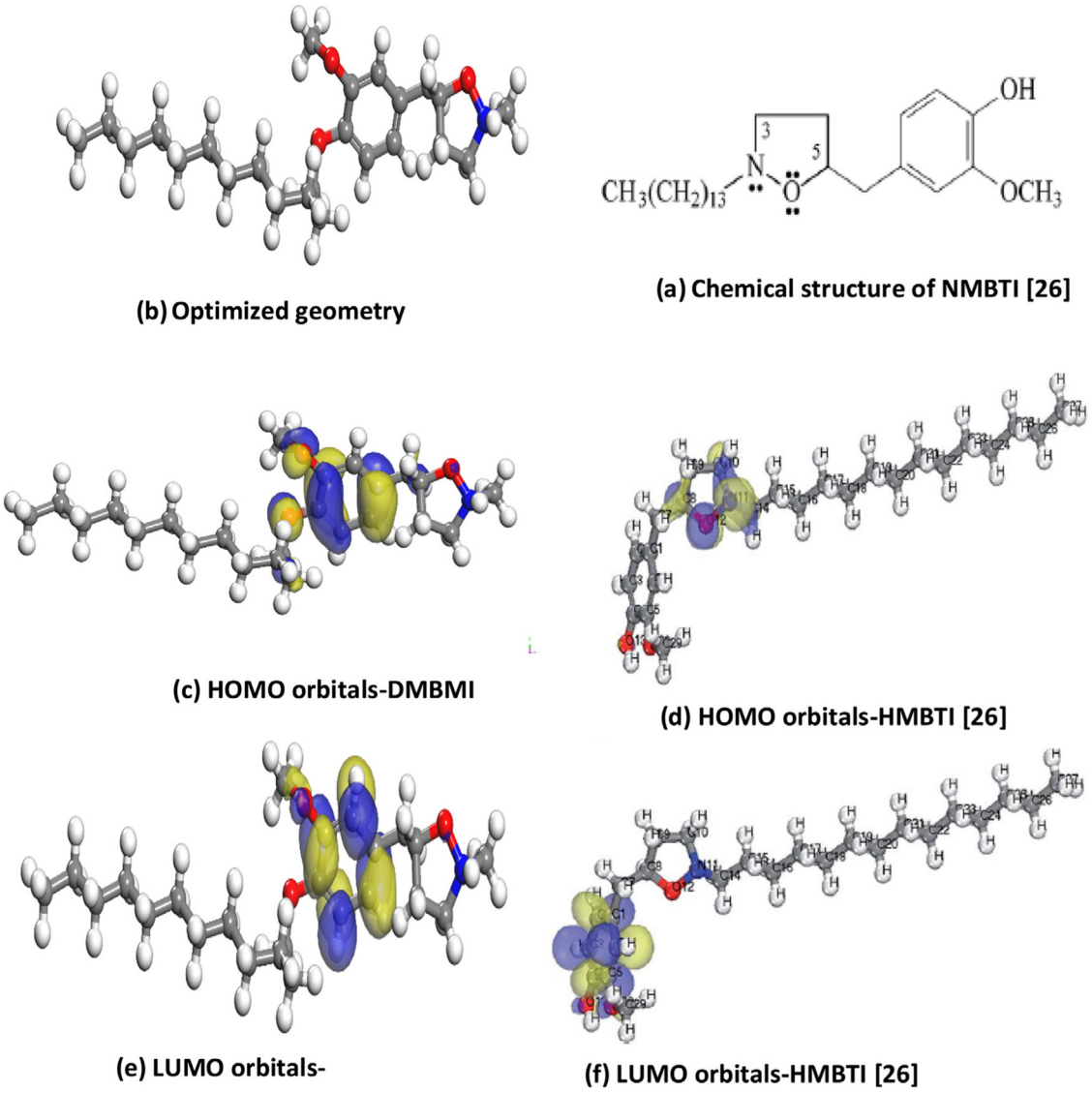

Fig. 4 – (a) Optimized structure, (c) HOMO and (e) LUMO orbitals distribution of protonated 5-(4-dodecyloxy-3-methoxybenzyl)-2-methylisoxazolidine (DMBMI-H$^+$); (b) chemical structure, (d), HOMO and (f) LUMO orbitals distribution of protonated of 5-(4-hydroxy-3-methoxybenzyl)-2-tetradecyl isoxazolidine (HMBTI). Figs. 4 (b, d, & f) were extracted from Alhaffar et al. [26]. Copyright The Royal Society of Chemistry 2018.

the HOMO and LUMO orbitals distribution presented in Fig. 4(c and e) were obtained. Clearly, the HOMO and LUMO orbitals are localized at the methoxybenzyl group. This infers that the methoxybenzyl group involves in a donor-acceptor interaction with the empty d-orbital of steel atom. This region is the active center for interaction of DMBMI molecules with the substrate surface.

3.3. *Monte Carlo simulations*

The interaction of DMBMI molecules with Fe (110) in the presence of 50 molecules of water were simulated using the Monte Carlo technique and the snapshot of the top views of the most stable configuration is shown in Fig. 5. The adsorbed DMBMI molecules assumed a parallel orientation with the Fe (110) surface. Such orientation can encourage maximal surface coverage and contact, which ensures strong interaction and in extension, effective corrosion inhibition. The adsorption energy of DMBMI on Fe (110) surface is −243.02 kcal/mol while that of H_2O adsorbed on Fe (110) surface is −11.96 kcal/mol. Clearly, the adsorption energy of DMBMI is significantly higher than that of water meaning DMBMI molecules have a higher tendency to displace adsorbed water molecules from the steel surface [28,30,31]. Again, the large adsorption energy of DMBMI signifies a very stable and strong interaction between DMBMI molecules and the metal surface [30,31].

It is believed that the higher the negative adsorption energy, the stronger the interaction of inhibitor molecules with a metal surface [26,30,31]. Alhaffar et al. [26] studied 5-(4-hydroxy-3-methoxybenzyl)-2-tetradecyl isoxazolidine (HMBTI) as inhibitor for API 5 L X60 steel in 1 mol/L HCl HCl solution. HMBTI (Fig. 4(b)) and DMBMI (Fig. 1) are isoxazolidine

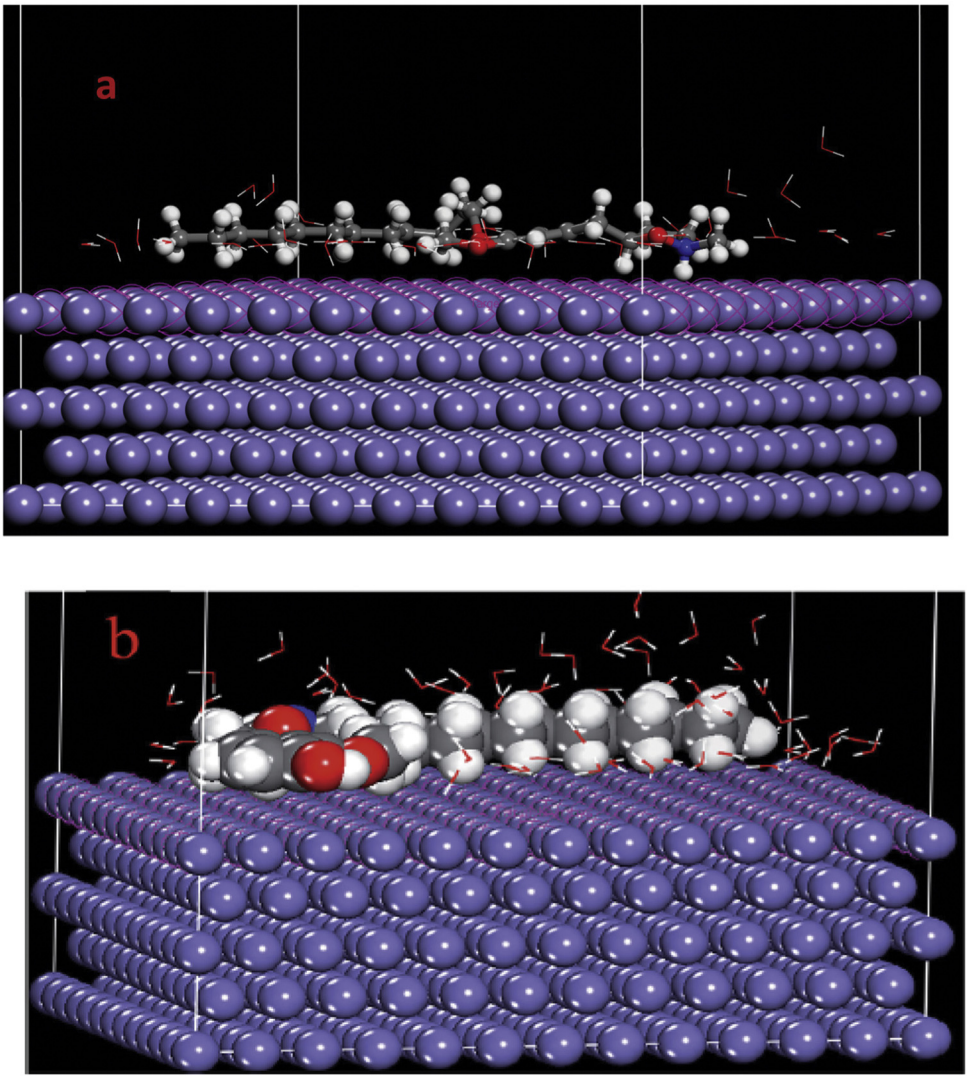

Fig. 5 – Top views of the most stable configurations for the adsorption of protonated (a) 5-(4-dodecyloxy-3-methoxybenzyl)-2-methylisoxazolidine (DMBMI-H$^+$) and (b) 5-(4-hydroxy-3-methoxybenzyl)-2-tetradecyl isoxazolidine (HMBTI) [26] on Fe (110) surface in the presence of 50 water molecules calculated using Monte Carlo simulations. Figs. 5 (b) was extracted from Alhaffar et al. [26]. Copyright The Royal Society of Chemistry 2018.

compounds that are similar in almost all aspect except the present of hydroxyl group in HMBTI. It was therefore appropriate to compare the results obtained by Alhaffar et al. [26] with the results from the present work. The HOMO and LUMO orbitals distribution reported by Alhaffar et al. [26] (Fig. 4(d and f)) clearly shows that the localization of electrons was same as in DMBMI (Fig. 4(c and e)), that is, electrons localization is at the methoxybenzyl group. However, Alhaffar et al. [26] reported inhibition efficiency of 67.7% at HMBTI concentration of 60 ppm (optimum) from electrochemical impedance spectroscopy technique whereas the same concentration for DMBMI gives inhibition efficiency of 61.9%. The Monte Carlo simulations of both HMBTI and DMBMI molecules on Fe (110) provides an insight into the slight differences in inhibitive performance of the two isoxazolidine compounds. While −269.81 kcal/mol was reported as the adsorption energy of HMBTI on Fe (110) surface [26], −243.02 kcal/mol is obtained for DMBMI, inferring stronger interaction of HMBTI molecules than DMBMI. By comparing Fig. 5(a) with Fig. 5(b), it is obvious that there was a stronger interaction between HMBTI molecules with the Fe surface than DMBMI.

3.4. *Experimental studies*

3.4.1. *Weight loss measurements*

The theoretical predictions portray DMBMI as a promising corrosion inhibitor. Experiments were therefore performed to validate the theoretical predictions. Weight loss measurement remains a simple, cost effective, and reliable experimental technique for studying the corrosion behavior of metals and inhibitive efficacy of metals corrosion inhibitors. Fig. 6 shows the variation of (a) corrosion rate of steel sample and (b) inhibition efficiency of various dosages of DMBMI at different temperatures. In Fig. 6(a), it is seen that the corrosion rate of API 5 L X60 steel decreased considerably in 1 mol/L HCl solutions containing DMBMI as inhibitor compared to the acid

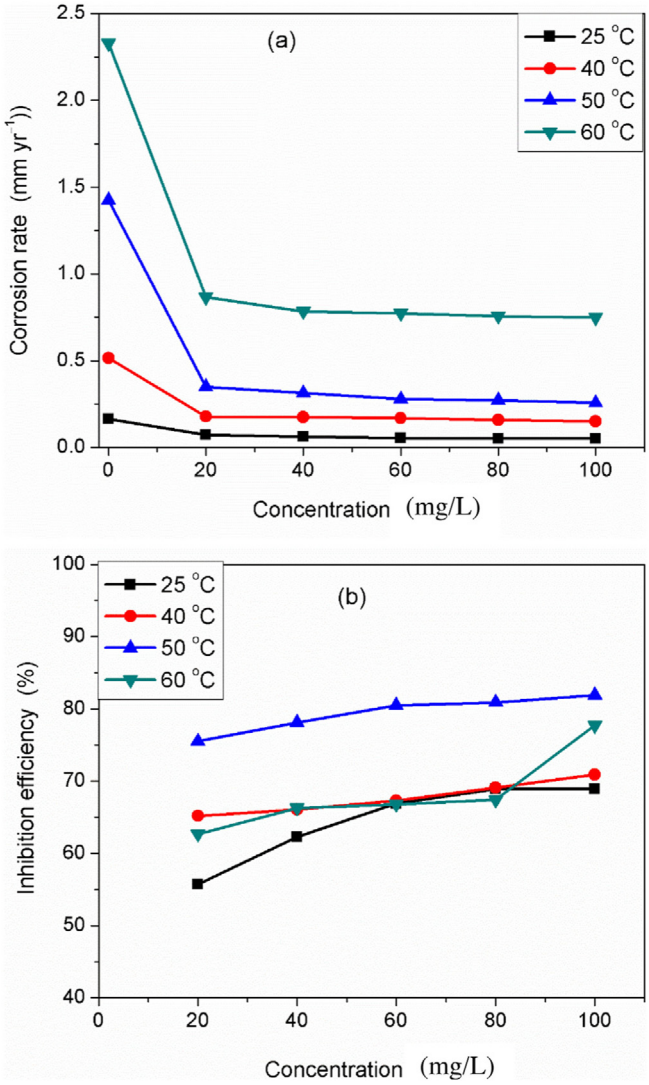

Fig. 6 – Graphs of (a) corrosion rate, (b) inhibition efficiency as a function of DMBMI concentration at different temperatures.

solution devoid of DMBMI at all the studied temperatures. This implies that, the presence of DMBMI in the acid solution retarded the dissolution of the metal. Also observed from Fig. 6(a) is the fact that, in both uninhibited and inhibited systems, corrosion rate increase with rise in system temperature. This means that the metal is susceptible to corrosion at elevated temperature. A careful inspection of Fig. 6(a) reveals that the corrosion rate is relatively constant within the inhibitor dosage of 40–100 mg/L at all temperatures. It seems that the optimum concentration of the inhibitor is within this range. In Fig. 6(b), the protection efficacy improves with increasing dosage of inhibitor up to 60 mg/L and thereafter slightly decline at all temperatures except 60 °C. Similar observation had been reported [26,32]. The possible explanation is that, as the inhibitor concentration was increased from 20 to 50 mg/L, the organic molecules were available for adsorption. At 60 mg/L (optimum concentration), maximum area of the metal surface was covered by the adsorbed inhibitor films. Beyond 60 mg/L, the system became saturated and adsorbed inhibitor species began to interact with free molecules. This led to film desorption and in extension, decline in inhibition efficiency [26,32]. The influence of temperature on the protection strength of DMBMI can also be visibly seen in Fig. 6(b). Corrosion retardation efficiency increased with rise in temperature up to 50 °C and decreased thereafter. The adsorbed inhibitor film may have dissolved at 60 °C.

In Table 2 is presented a comparative analysis of the corrosion inhibition performance of DMBMI with some isoxazolidine derivatives reported [9–12,26]. It is clear from the table that isoxazolidine-based inhibitors are promising for low carbon steel in HCl environment. However, some disparities in inhibition performance are observed. For instance, the inhibition efficiency values obtained in the present work and that of Alhaffar et al. [26] are lower. As it is known, the adsorption of organic inhibitors *vis-à-vis* inhibition effectiveness is influenced by factors such as the chemical structure of the inhibitor, the metal surface charge, the distribution of charge in the molecule, the type of aggressive medium (pH and/or electrode potential), *etc.* [33]. The observed disparity may not be far from the influence of some or all of these factors.

The performance of a good corrosion inhibitor is anchored on its adsorption strength on the metal surface. Hence, the important information about the nature of metal-inhibitor interaction can be derived from adsorption isotherm. Against this back drop, the degree of surface coverage values ($\theta = \eta/100$) (assuming inhibition efficiency varies linearly with degree of surface coverage) for various DMBMI concentrations were computed to present the best adsorption isotherm. The computed θ values were fitted into various adsorption isotherms models, including Frumkin, Temkin, Freundlich and Langmuir adsorption isotherms. The best fit isotherm was noted for Langmuir based on the values of correlation coefficient (R^2) (Table 3). This isotherm is defined by:

$$\frac{C_{inh}}{\theta} = \frac{1}{K_{ads}} + C_{inh} \quad (1)$$

where θ is the surface coverage, K_{ads} is the equilibrium constant of the adsorption process, and C_{inh} is the concentration of DMBMI. By plotting C_{inh}/θ as a function of C_{inh}, straight line graphs given in Fig. 7(a) were obtained. The slopes of the graphs deviated slightly from unity (Table 3) expected from an ideal Langmuir isotherm graph. This suggests possible interaction among adsorbed species [34]; a vital factor that was ignored during the derivation of Langmuir equation.

To verify if there was interaction in the adsorbed layer on the metal surface, El-Awady et al. kinetic-thermodynamic model, which takes into consideration, interaction of adsorbed species [35] was employed. The El-Awady et al. kinetic-thermodynamic isotherm assumes the form:

$$\log\left(\frac{\theta}{1-\theta}\right) = \log K_{ads} + y \log C_{inh} \quad (2)$$

where 1/y represents the number of active sites occupied by inhibitor or the number of water molecules substituted by an inhibitor molecule [36]. The value of 1/y greater than unity implies interaction of adsorbed molecules [37]. Fig. 7(b) shows the El-Awady et al. kinetic-thermodynamic isotherm plots

Table 2 – A comparison of the inhibitive performance of isoxazolidine-based derivatives for low carbon steel in HCl medium from Weight Loss measurement technique/.

S/N	Inhibitor (Inh.)	Tempt. (°C)	Inhibitor conc.	η (%)	Ref.
1	2-Decylhexahydropyrrolo[1,2-b]isoxazole	60	50	98.0	[9]
2	3-Tetradecylhexahydropyrrolo[1,2-b]isoxazole		ppm	97.5	
3	N,N-di(hexahydropyrrolo[1,2-b]isoxazole2-ylmethyl)-N^1-formyl-1,12-dodecanediamine			97.0	
4	N,N-di(hexahydropyrrolo[1,2-b]isoxazole-2-ylmethyl)-1,12-dodecanediamine			95.2	
5	2-methyl-5-hexylisoxazolidine	60	1200 ppm	86.0	[10]
6	2-methyl-5-dodecylisoxazolidine		200 ppm	93.7	
7	2-isopropyl-5-dodecylisoxazolidine		25 ppm	92.5	
8	2-tert-butyl-5-dodecylisoxazolidine		10 ppm	90.1	
9	1-(2,3-diphenyl-isoxazolidin-5-yl)-nonan-2-ol	25	50 ppm	83.9	[11]
10	5-octylsulfanylmethyl-2,3-diphenylisoxazolidine		50 ppm	91.0	
11	9-(2,3-diphenyl-isoxazolidin-5-yl)-nonanoic acid 2-[2-(2-methoxy-ethoxy)-ethoxy]-ethyl ester		50 ppm	88.6	
12	2-(9-phenoxynonyl)hexahydropyrrolo [1,2 b]isoxazole	60	100 ppm	92.0	[12]
13	2-(9-p-methoxyphenoxynonyl) hexahydropyrrolo [1,2-b] isoxazole		100 ppm	85.0	
14	2-(9-phenoxynonyl)hexahydro-2Hisoxazolo[2,3-a] pyridine		100 ppm	97.0	
15	2-(9-p-methoxyphenoxynonyl) hexahydro-2H-isoxazolo[2,3-a]pyridine		100 ppm	90.0	
16	5-(benzo[d][1,3]dioxol-5-ylmethyl)-2-tetradecyl isoxazolidine	60	60 ppm	79.5	[21]
17	5-(4-hydroxy-3-methoxybenzyl)-2-tetradecyl isoxazolidine		60 ppm	82.3	
18	5-(4-dodecyloxy-3-methoxybenzyl)-2-methylisoxazolidine	25	60 ppm	66.9	Present work
		60	60 ppm	66.8	

Table 3 – Langmuir adsorption parameters for carbon steel in 1 mol/L HCl containing DMBMI from weight loss measurements at different temperatures.

Temperature(°C)	Langmuir				El-Awady et al.	
	ΔG^{o}_{ads} (kJ mol^{-1})	K_{ads}	Slope	R^2	1/y	R^2
25	–35.30	1.53	1.59	0.963	2.67	0.963
40	–32.82	0.30	1.38	0.998	6.25	0.788
50	–32.91	0.21	1.19	0.999	4.29	0.963
60	–31.76	0.10	1.26	0.967	6.72	0.917

for the adsorption of DMBMI onto the carbon steel surface in the studied corrosive medium. The R^2 values are slightly lower than those from the Langmuir isotherm (Table 3) but within the range that allows the model to be used to describe the adsorption process. It is obvious that DMBMI adsorbed molecules occupied more than one active site on the metal surface. As could be seen in Table 3, 1/y is greater than unity.

The K_{ads} values listed in Table 3 were computed from the intercepts of the plots in Fig. 7(a). K_{ads} value defines the strength of the bond between adsorbate and adsorbent [38]. Large K_{ads} value implies strong adsorption bond and small K_{ads} value infers the opposite. Our K_{ads} value is low and decrease with rise in temperature (Table 3). This is typical of a physisorption kind of adsorption [34]. The K_{ads} is related to the standard free energy of adsorption (ΔG^0_{ads}) thus [38,39]:

$$\Delta G^0_{ads} = -RT \ln\left(1 \times 10^6 K_{ads}\right) \quad (3)$$

where 1×10^6 is the concentration of water molecules (same as concentration of inhibitor) in mg/L, R and T are the molar gas constant and absolute temperature respectively. The calculated ΔG^0_{ads} values are given in Table 3 and fall within the range often associated with mixed adsorption (both physical and chemical) mechanism in the corrosion literature [38,39]. The standard free energy for the adsorption can be linked to the standard enthalpy (ΔH^0_{ads}) and entropy (ΔS^0_{ads}) of the adsorption as follows [38,40]:

$$\Delta G^0_{ads} = \Delta H^0_{ads} + T\Delta S^0_{ads} \quad (4)$$

A combination of Eqs. (3) and (4) and rearrangement of the resultant equation gives,

$$\ln K_{ads} = \frac{-\Delta H^0_{ads}}{RT} + \frac{\Delta S^0_{ads}}{R} - \ln\left(1 \times 10^6\right) \quad (5)$$

Fig. 7(b) shows the plot of $\ln K_{ads}$ versus $1/T$ for the studied systems. The ΔH^0_{ads} and ΔS^0_{ads} values calculated from the slope ($\Delta H^0_{ads}/R$) and intercept (($\Delta S^0_{ads}/R$) – $\ln(1 \times 10^6)$) respectively are – 36.72 kJ/mol and – 12.93 kJ/mol. As it is known, positive value of ΔH^0_{ads} is indicative of endothermic process while negative value means exothermic process [38,40]. For an endothermic adsorption process, ΔH^0_{ads} value greater than zero is interpreted as chemical adsorption while ΔH^0_{ads} value less than

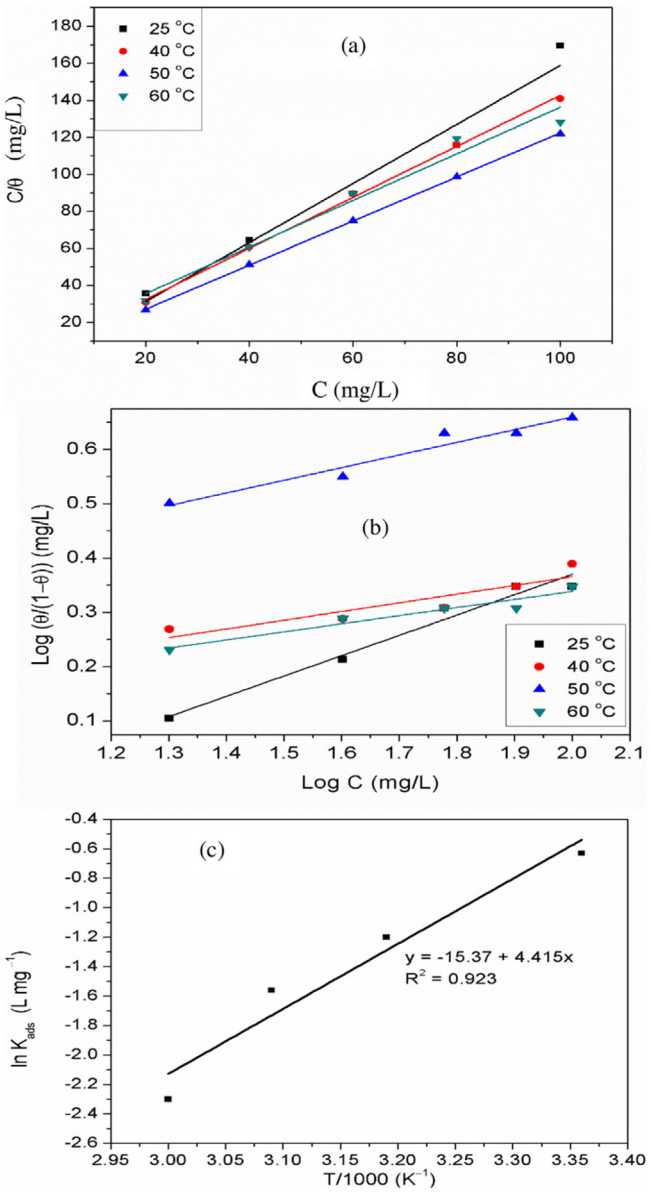

Fig. 7 – (a) Langmuir adsorption isotherm plots at different temperatures, (b) El-Awady et al. kinetic-thermodynamic isotherm plots, and (c) graph of ln K_{ads} vs. 1/*T* for DMBMI adsorption on API 5 L X60 steel in 1 mol/L HCl.

zero implies physical adsorption [25,38]. Similarly, when the adsorption process is exothermic in nature, ΔH^0_{ads} value less than 40 kJ/mol points to physical adsorption whereas ΔH^0_{ads} value near 100 kJ/mol signifies chemical adsorption [38,40]. For the system under consideration, the ΔH^0_{ads} is negative implying that the adsorption of DMBMI molecules onto the steel surface was exothermic in nature. The magnitude of the ΔH^0_{ads} (36.72 kJ/mol) is less than 40 kJ/mol and at the same time very close to chemisorption benchmark. This can be interpreted as mixed adsorption type (i.e both physical and chemical adsorption mechanisms) but with the dominant mechanism being physisorption [40]. The ΔS^0_{ads} value is negative and could be interpreted to mean less perturbation in the inhibited systems [38,41].

Table 4 – Activation parameters for carbon steel in 1 mol/L HCl in the absence and presence of different concentrations of DMBMI.

Concentration(mg/L)	E_a(kJ mol^{-1})	ΔH^*(kJ mol^{-1})	$-\Delta S^*$(J mol^{-1} K^{-1})
Blank	63.39	60.23	57.82
20	55.97	53.23	88.74
40	56.90	54.17	86.59
60	59.26	56.61	79.50
80	59.77	57.58	76.83
100	52.69	50.58	98.66

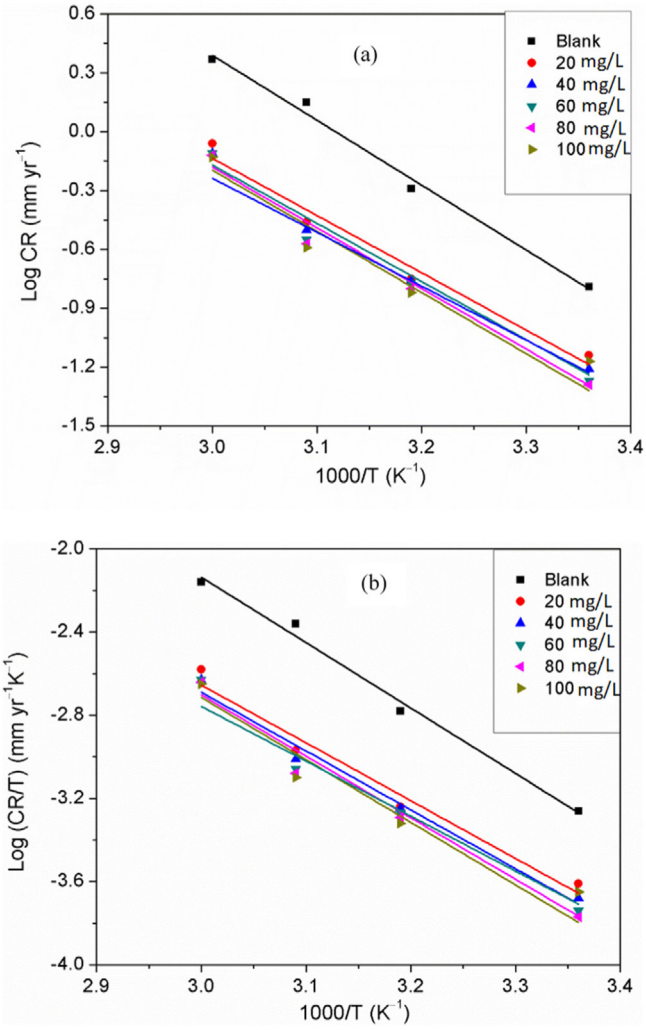

Fig. 8 – (a) Arrhenius and (b) Transition state plots for API 5 L X60 steel in 1 mol/L HCl in the absence and presence of different concentrations of DMBMI.

It is obvious in Fig. 6 that temperature has a significant effect on the corrosion behavior of API 5 L X60 steel in 1 mol/L HCl without and with DMBMI. The corrosion kinetics parameters such as activation energy (E_a), activation enthalpy (ΔH^*), and activation entropy (ΔS^*) were calculated from the Arrhenius (Eq. 6) and Transition State (Eq. 7) equations and are listed in Table 4. Fig. 8 depicts the Arrhenius and Transition state

plots for the steel in acid medium devoid of and containing different concentrations of DMBMI.

$$\text{Log}\upsilon = \log A - \left(\frac{E_a}{2.303RT}\right) \quad (6)$$

$$\text{Log}\left(\frac{\upsilon}{T}\right) = \left[\left(\log\left(\frac{R}{Nh}\right) + \left(\frac{\Delta S^*}{2.303R}\right)\right)\right] - \frac{\Delta H^*}{2.303RT} \quad (7)$$

where υ is the corrosion rate, A is the frequency factor, N the Avogadro's number, and h is the Planck's constant. The E_a values of the DMBMI inhibited systems presented in Table 4 are smaller than that of uninhibited solution. This infers a chemisorption mechanism [38]. However, it is observed that the difference between the inhibited E_a values and that of the uninhibited is slim suggesting that both physisorption and chemisorption mechanisms were in place on the metal surface. It was suggested [42] that adsorption should not be considered as mere physical or chemical, since there is no distinct differentiation line between these two adsorption mechanisms. Authors [42–44] held that the two mechanisms are not separate but one being a preceding step to another. It is also noticed in Table 4 that the ΔH^* value is opposite to the ΔH^0_{ads} (i.e., ΔH^* has a positive value whereas ΔH^0_{ads} has a negative value). It means that, while the adsorption of the inhibitor molecules onto the steel surface was exothermic, the activation step of the corrosion process was endothermic in nature [45]. The ΔS^* values are negative and large. Most often, negative and large value of ΔS^* is associated with the activated complex in the rate determining step representing an association rather than a dissociation [38,45]. More so, the magnitude of the inhibited ΔS^* values are bigger compared to that of uninhibited and this signifies increase in solvent entropy occasioned by water desorption from the substrate surface [45].

The optimum concentration of DMBMI afforded corrosion inhibition efficiency of 66.9% and 66.8% at 25 °C and 60 °C, respectively (Fig. 6). By these values, DMBMI could be placed under moderate corrosion inhibitors. We therefore took step towards enhancing the corrosion inhibition performance of this eco-friendly compound. The capability of iodide ions in boosting the anticorrosive property of organic compounds have been widely reported [46–48]; this modification approach was therefore adopted. In Table 5 is given the corrosion rate, surface coverage, and η values obtained for specimen in the corrodent containing either 60 mg/L DMBMI, 0.005 mol/L KI, or their mixtures at 25 °C and 60 °C from weight loss experiments. Obviously, the addition of KI to DMBMI benefitted the inhibition efficiency remarkably particularly at elevated temperature. For instance, the inhibition efficiency of the compound was upgraded from 66.9% and 66.8% to 74.5% and 91.6% at 25 °C and 60 °C respectively. As earlier mentioned, iodide ions boost the corrosion retardation strength of organic inhibitor by co-adsorption which could be cooperative or competitive [46–48]. These two kinds of co-adsorption can be differentiated using the value of the synergism parameter (S_1). S_1 value greater than or equal to unity indicates cooperative co-adsorption while S_1 value less than unity is consistent with competitive co-adsorption [46]. The value of S_1 at 25 °C and 60 °C (Table 5), calculated using equation given in Ref. [49], are less than unity meaning DMBMI and iodide ions competitively adsorbed onto carbon steel surface in the considered medium.

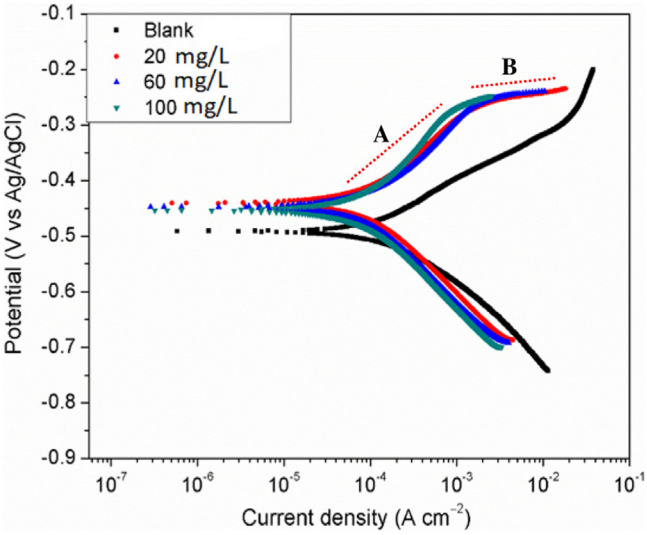

Fig. 9 – Potentiodynamic polarization plots for API 5 L X60 steel without and with different concentrations of DMBMI at 25 °C.

3.4.2. *Electrochemical measurements*

The potentiodynamic polarization curves obtained for the steel in 1 mol/L HCl solution without and with selected concentrations of DMBMI are shown in Fig. 9. The values of corrosion potential (E_{corr}), corrosion current density (i_{corr}), and anodic and cathodic Tafel slopes (β_a and β_c) derived by extrapolating the linear segments of the graphs in Fig. 9 are given in Table 6. The inhibition efficiency (η) value also presented in the table was calculated using the equation given in Ref. [47]. By visually examining Fig. 9, the following observations are made: (i) in the polarization graph of the blank, a direct relationship between the corrosion current density and the corrosion potential is observed in the anodic region. This is indicative of the active dissolution of the metal in the studied environment [50,51]. (ii) The presence of DMBMI in the acid solution affected the polarization pattern of the metal specimen. This is evident in the reduction of the cathodic and anodic current densities to lower values and the shifting of the corrosion potential towards anodic direction relative to that of the blank. (iii) In the anodic polarization curves recorded in inhibited systems, two sections designated as A and B are identified; they represent the inhibited and uninhibited regions [52], respectively. (iv) The inhibitor has greater influence on the anodic reactions than cathodic reactions. In Table 6, it is observed that the E_{corr} values of inhibited systems are nobler than that of uninhibited. This, and the observations made from Fig. 9 can be interpreted to mean that DMBMI functioned in the studied system principally as an anodic type inhibitor. Further inspection of the results in Table 6 disclose that i_{corr} values obtained for inhibited systems are smaller than that of uninhibited. The value further decreased with increasing inhibitor concentration and, as a result, the inhibition efficiency increased. This indicates an increase in the

Table 5 – Corrosion rate and inhibition efficiency values for carbon steel in 1 mol/L HCl containing DMBMI, KI and DMBMI – KI mixtures at 25 and 60 °C from weight loss measurements.

Temperature (°C)	System/concentration	Corrosion rate (mm/yr)	Inhibition efficiency (%)	Surface coverage (θ)	Synergistic parameter (S_1)
	Blank	0.164	–	–	
25	DMBMI (60 mg/L)	0.054	66.9	0.67	
	KI (0.005 mol/L)	0.079	51.9	0.52	0.63
	DMBMI + KI	0.0042	74.5	0.75	
	Blank	2.327			
60	DMBMI (60 mg/L)	0.774	66.8	0.67	
	KI (0.005 mol/L)	0.444	80.9	0.81	0.78
	DMBMI + KI	0.0195	91.6	0.92	

Table 6 – Potentiodynamic polarization (PDP) and Linear polarization resistance (LPR) parameters for carbon steel in 1 mol/L HCl without and with selected concentrations of DMBMI at 25 °C.

			PDP method			LPR method	
Concentration (mg/L)	E_{corr} (mV/Ag/AgCl)	i_{corr} (μA cm^{-2})	β_a (mV dec^{-1})	β_c (mV dec^{-1})	η (%)	R_p (Ω cm^2)	η (%)
Blank	–491	158.0	129.5	112.6	–	189.6	–
20	–441	120.0	175.8	179.8	24.1	338.1	43.9
60	–436	98.3	174.9	205.9	37.8	409.1	53.7
100	–438	92.5	143.7	194.4	41.5	437.3	56.6

blocked fraction of the metal surface by adsorption [53] as the concentration of the inhibitor was increased. Again, the β_a and β_c values of inhibited systems are bigger than values obtained in the uninhibited system. This shows that the adsorption film of DMBMI on the metal surface interrupted both the anodic and cathodic corrosion reactions [54,55]. But from Fig. 9, the dominant effect is on the anodic dissolution reactions.

It is worth pointing out that, the theoretical prediction is in perfect agreement with the results from potentiodynamic polarization (PDP) measurements. For instance, theoretically, we predicted that DMBMI is mostly in protonated form (Fig. 3). The PDP results (Fig. 9; Table 6) show that DMBMI is principally an anodic type inhibitor. The mechanism of anodic dissolution of iron in HCl solution is as follow [56,57]:

$$Fe + Cl^- \leftrightarrow \left(FeCl^-\right)_{ads} \quad (8)$$

$$\left(FeCl^-\right)_{ads} \leftrightarrow (FeCl)_{ads} + e^- \quad (9)$$

$$(FeCl)_{ads} \rightarrow \left(FeCl^+\right) + e^- \quad (10)$$

$$\left(FeCl^+\right) \leftrightarrow Fe^{2+} + Cl^- \quad (11)$$

The corresponding cathodic hydrogen evolution reactions are:

$$Fe + H^+ \leftrightarrow \left(FeH^+\right)_{ads} \quad (12)$$

$$\left(FeH^+\right)_{ads} + e^- \rightarrow (FeH)_{ads} \quad (13)$$

$$FeH_{ads} + H^+ + e^- \rightarrow Fe + H_2 \quad (14)$$

The $DMBMI^+$ will favorably adsorb on the anodic site than the cathodic site according to the following reaction:

$$\left(FeCl^-\right)_{ads} + DMBMI^+ \rightarrow \left(FeCl^-DMBMI^+\right)_{ads} \quad (15)$$

Linear Polarization Resistance (LPR) technique was also adopted in the study of the corrosion and corrosion inhibition of API 5 L X60 steel in 1 M HCl solution without and with DMBMI. The values of the polarization resistance (R_p) and inhibition efficiency are also presented in Table 6. It is clear in the table that R_p increase in inhibited acid solutions compared to the uninhibited solution signifying that DMBMI suppressed the steel deterioration in the corrosive acid environment. The trend of inhibition efficiency in PDP and LPR with concentration is somewhat different from that noted in weight loss measurements (Fig. 2), that is, 60 mg/L is not the optimum concentration. Nevertheless, the inhibition efficiency for 60 mg/L and 100 mg/L are in close range. For instance, in LPR, 60 mg/L DMBMI afforded 53.7% while 100 mg/L offered 56.6%. It could therefore be economical to utilize the 60 mg/L concentration.

Fig. 10 presents the impedance recorded for API 5 L X60 steel in 1 M HCl solution in the absence and presence of selected concentrations of DMBMI at 25 °C exemplified as (a) Nyquist, (b) Bode modulus, and (c) Phase angle formats. In the uninhibited acid solution, the impedance graph recorded is characterized by single capacitive loop at high frequencies. However, in the impedance graphs for inhibited systems, an unresolved capacitive loop is observed at medium frequencies in addition to the capacitive loop at high frequencies pointing to two times constant. The two time constants could arise from the double layer structure of the DMBMI adsorbed film on the steel surface [58,59]. The capacitive loop observed at high frequencies in the impedance diagram recorded in free acid solution defined the charge transfer resistance of the steel electrode [54]. The semicircles at high frequencies in inhibited impedance diagrams represent the polarization resistance between the metal and HCl solution interface [54]. According to some authors [60], this polarization resistance encompasses all the resistances (charge transfer resistance, film resistance, diffuse layer resistance, accumulation resistance, *etc.*) between metal and solution interface. Compared

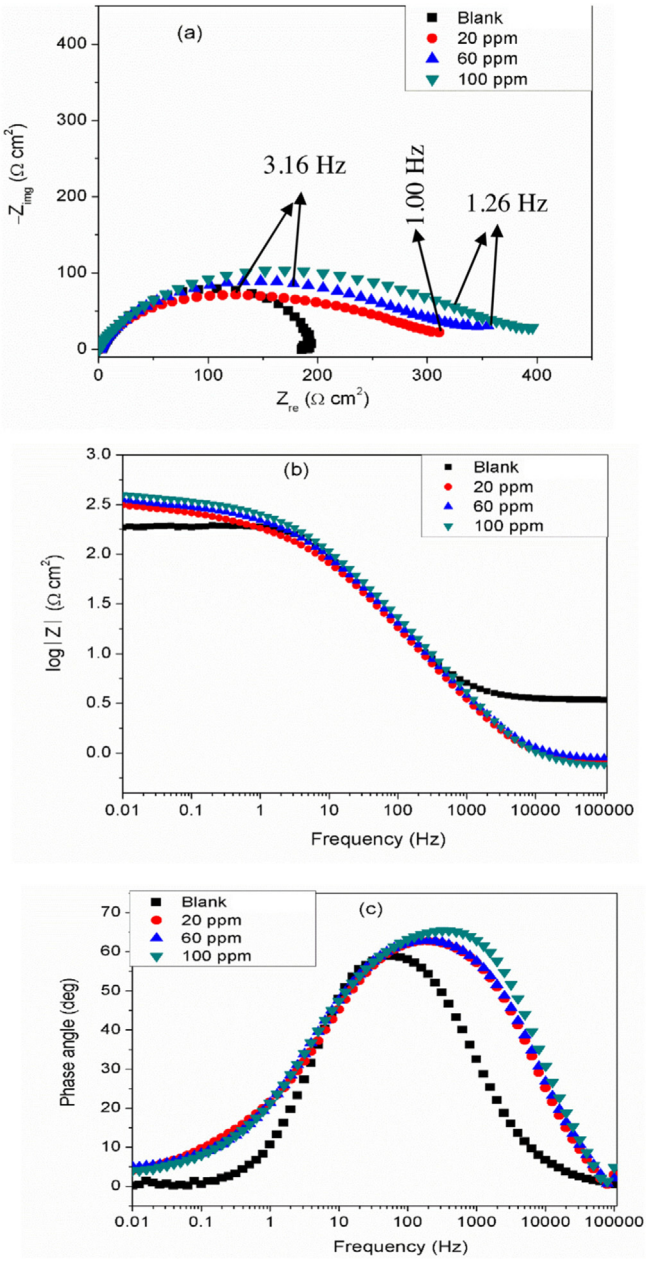

Fig. 10 – Impedance plots for API 5 L X60 steel in 1 mol/L HCl without and with selected concentrations of DMBMI exemplified as (a) Nyquist, (b) Bode modulus, and (c) Phase angle formats at 25 °C.

with that of the uninhibited, the semicircles in impedance diagrams recorded in inhibited acid solutions are bigger, meaning lesser corrosion of the steel specimen in inhibited solutions. This is also manifested in the Bode modulus and Phase angle plots. For instance, the Z_{mod} and Phase angle are displaced towards bigger values (Fig. 10(b) and (c)). However, all the semicircles in Fig. 10(a) are far from being perfect semicircles; a phenomenon often linked with frequency dispersion and microscopic roughness of working electrode surface [54,56]. Increase in inhibitor concentration is found to increase the size of the capacitive loop, shift absolute values of Bode modulus and Phase angle to higher values. This implies that, the resistance of the substrate varied proportionately with inhibitor concentration probably due to increase in surface coverage by protective film.

The fitting of the impedance data was achieved using the equivalent circuits (EC) inserted in Fig. 11. The EC inserted in Fig. 11(a) was used for data from uninhibited acid solution while data from inhibited solutions were fitted using the EC inserted in Fig. 11(b). As could be seen in Fig. 11, good fit was achieved with these ECs. The ECs have the following elements in common: solution resistance (R_s), charge transfer resistance (R_{ct}), and constant phase element (CPE) which was necessary because of the imperfectness of the obtained impedances. In addition, the EC in Fig. 11(b) has the film resistance (R_f) element. The ECs gave excellent fitting as evident in the low chi squared values (Table 7) and fitting errors, which were all less than 5%. All the impedance parameters associated with the studied systems are listed in Table 7. Inhibition efficiency was calculated using the equation given in Ref. [26]. From the results presented in Table 7, it is seen that the presence of DMBMI in the acid solution caused the solution resistance to decrease but raised the polarization resistance of the substrate. The presence of 100 mg/L of the inhibitor raised the steel resistance from 192.9 Ω cm^2 to 622.6 Ω cm^2 and this corresponds to inhibition efficiency of 69.0%. Judging from the values of n_1, the surface of API 5 L X60 steel behaved as a capacitor in 1 mol/L HCl solution.

3.4.3. *Surface assessments*

Fig. 12 shows the SEM/EDAX pictures taken for the studied substrate (a) in abraded state, (b, c) exposed to corrosive solution, (d, e, f) exposed to corrodent containing DMBMI (60 mg/L), and (g, h) exposed to corrodent containing 60 mg/L DMBMI +0.005 mol/L KI at 25 °C for 24 h. After mechanical abrasion, the surface of the metal specimen was smooth as could be seen in Fig. 12(a). Immersion in 1 mol/L HCl left the surface seriously damaged. The surface assumed a rough and coarse morphology (Fig. 12(c)). It is seen from Fig. 12(c) that the metal surface was covered with corrosion products and the EDAX spectrum in Fig. 12(b) reveals that the products was rich in chloride (16.8 wt.%). This is in agreement with the anodic oxidation reaction given in Eq. 7. Obviously, the corrosion mitigation of the steel specimen in the studied acid solution fortified with DMBMI was due to adsorption mechanism. In Fig. 12(e), the adsorbed film appears as black spot. The EDAX scan of the entire surface (Fig. 12(d)) discloses that the concentration of chloride on the surface was greatly reduced compared to the surface in Fig. 12(b). That is, the concentration declined from 16.8% to 8.3%. As suggested by Eq. 15, $DMBMI^+$ ions are adsorbed on $\left(FeCl^-\right)_{ads}$ to form $\left(FeCl^-DMBMI^+\right)_{ads}$. The concentration of chloride on the surface in Fig. 12(e) is expected to be less relative to the surface in Fig. 12(c). To confirm that the black spot was actually adsorbed DMBMI film, EDAX analysis was performed on the spot and the spectrum is shown in Fig. 12(f). Obviously, the deposit is of DMBMI. The C and O concentrations are very high, that is, 10.9 and 10.5% respectively. These are elemental components of the DMBMI. The Cl concentration is also high at this spot (i.e., 29.8%). This again confirms that the polycations are adsorbed on a layer of chloride ions. The best surface protection was achieved with DMBMI + KI mixture, which is in perfect agreement with the

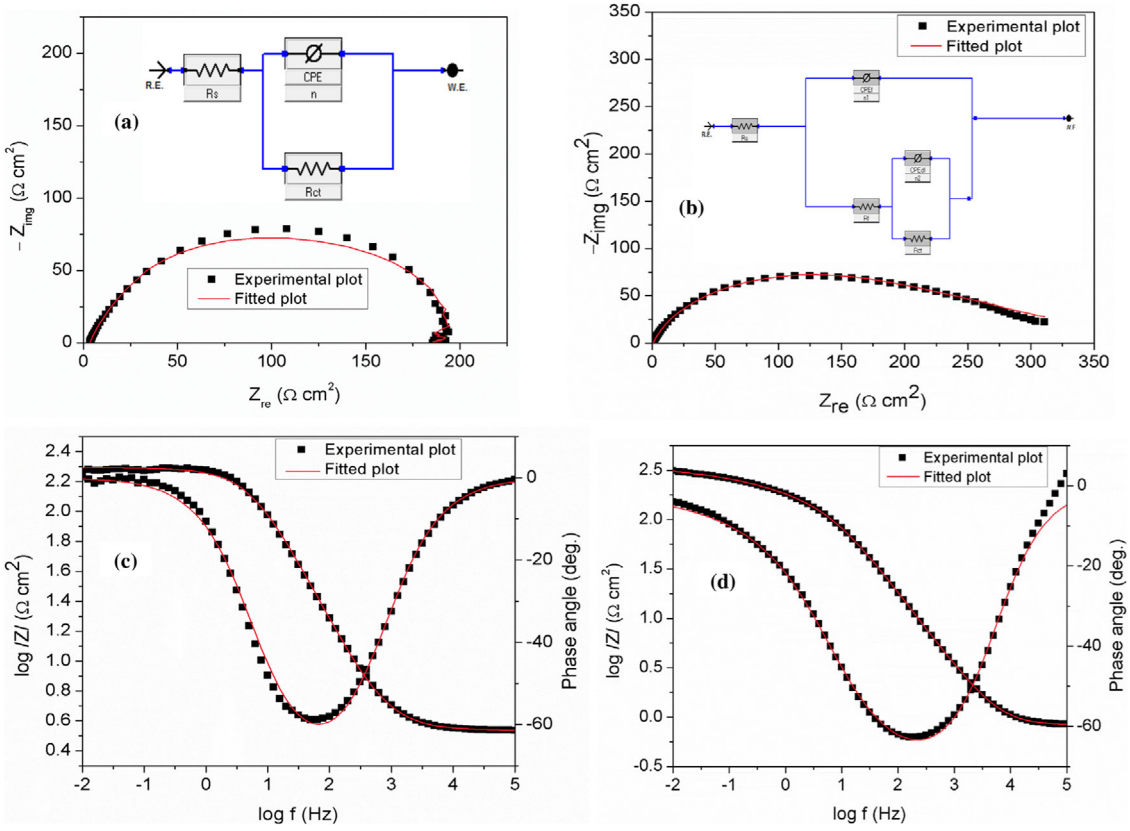

Fig. 11 – Experimental and fitted impedance data of St37 steel (a,c) in the absence and (b,d) in the presence of DMBM at 298 K. The respective equivalent circuits used for the fitting are inserted in (a) and (b).

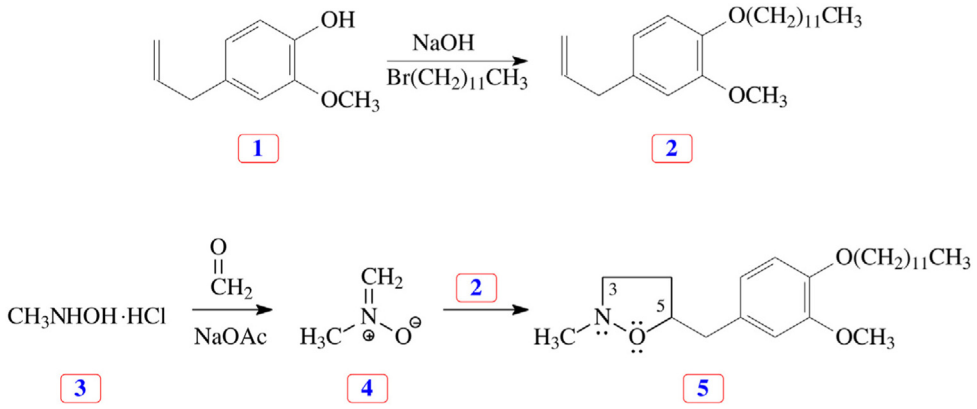

Scheme 1 – Synthesis of inhibitor molecule 5 using nitrone cycloaddition reaction.

experimental results (Table 5). As could be seen in Fig. 12(g), less damage was done to the surface compared to the surface in Fig. 12(c & e). On this surface, the Cl concentration was low (3.5 wt.%). As it is known, in a system containing iodide and chloride ions, iodide ions would be predisposed to adsorption than chloride ions because of higher ionic radius [20].

To further explain the interaction of DMBMI molecules with the steel surface, the films extracted from the specimen surface after exposing to the inhibited acid solutions were analyzed spectroscopically. Fig. 13 shows the comparative FTIR spectra of pure DMBMI and adsorbed films extracted from API 5 L X60 steel surface. Inspection of Fig. 13 reveals that the O heteroatoms in the pendant groups attached to the benzene ring and the heterocyclic N and O heteroatoms (Scheme 1) participated in the adsorption process. In the FTIR spectrum of pure DMBMI (Fig. 13(a)), the strong peaks at 2917.50 and 2850.08 cm^{-1} are attributed to the ring C–N stretching [61]. The bands at 1589.91 and 1512.91 cm^{-1} emanated from the ring N–O vibrations [61] while the peak at 1232.31 cm^{-1} originated from the C–O vibration of the benzene pendant groups. By comparing Fig. 13(a) to Fig. 13(b) and (c), it could be seen that these peaks diminished completely pointing to the involvement of these heteroatoms in the adsorption process. These findings are in perfect agreement with the theoretical prediction in Fig. 4.

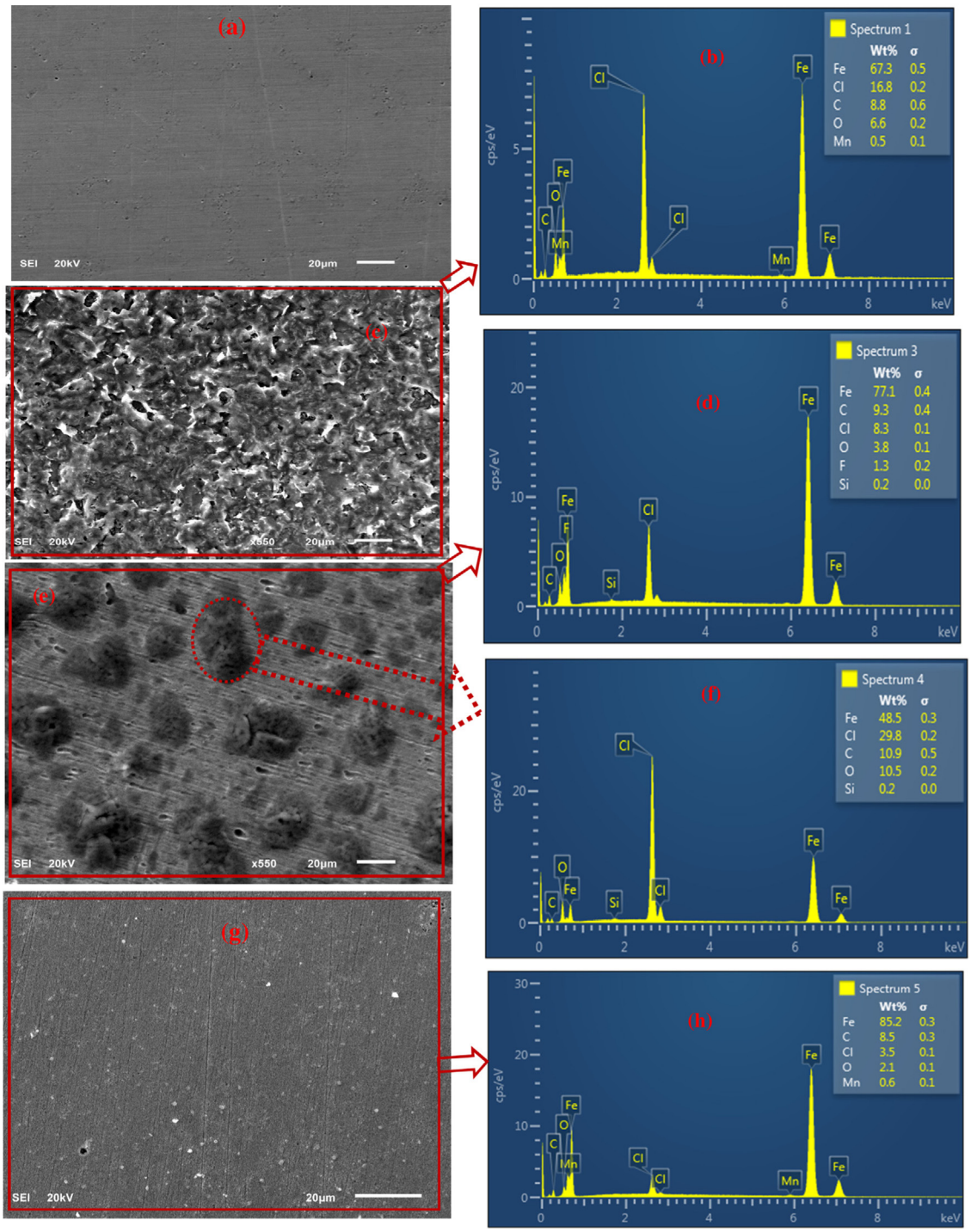

Fig. 12 – SEM pictures and EDAX images for API 5 L X60 steel (a) in abraded state (b, c) exposed to 1 mol/L HCl solution (d, e, f) exposed to 1 mol/L HCl solution containing DMBMI (60 mg/L), and (g, h) exposed to 1 mol/L HCl solution containing 60 mg/L DMBMI +0.005 mol/L KI at 25 °C for 24 h.

Table 7 – Impedance parameters for low carbon steel in 1 mol/L HCl without and with selected concentrations of DMBMI at 25 °C.

Concentration (mg/L)	R_s (Ω cm^2)	CPE_f		R_f (Ω cm^2)	CPE_{dl}		R_{ct} (Ω cm^2)	R_p (Ω cm^2)	$\chi^2 \times 10^{-3}$	η (%)
		Y_o ($\mu\Omega$ s^n cm^{-2})	n1		Y_o (Ω s^n cm^{-2}) $\times 10^{-3}$	n2				
Blank	3.44 ± 0.11	0.27	0.82	—	—	—	192.9	—	1.0	–
20	0.82 ± 0.12	254.3	0.82	0.001 ± 0.00	1.40	0.27	378.3 ± 3.58	378.30	0.85	49.0
60	0.77 ± 0.10	219.7	0.81	4.42 ± 0.01	1.24	0.27	502.0 ± 2.93	506.42	0.78	61.9
100	0.84 ± 0.10	302.8	0.78	9.93 ± 0.03	1.89	0.13	612.7 ± 3.11	622.63	0.85	69.0

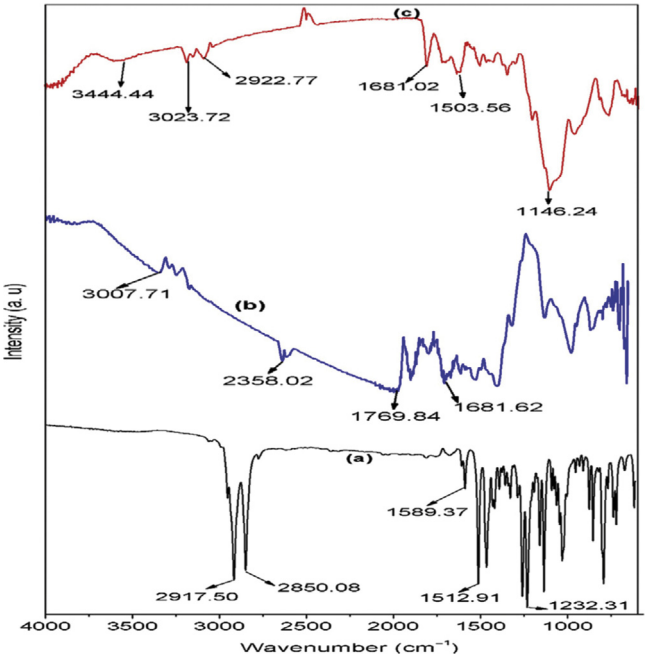

Fig. 13 – FTIR spectra of (a) pure DMBMI, (b) adsorbed film extracted from API 5 L X60 steel surface exposed to 1 mol/L HCl solution containing 60 mg/L DMBMI, and (c) adsorbed film extracted from API 5 L X60 steel surface exposed to 1 mol/L HCl solution containing 60 mg/L DMBMI +0.005 mol/L KI for 24 h at 25 °C.

4. Summary and conclusions

A new compound, 5-(4-dodecyloxy-3-methoxybenzyl)-2-methylisoxazolidine (DMBMI) has been successfully synthesized and characterized spectroscopically. The compound is nontoxic, has good solubility property, and exist in protonated form in acid solution of pH = 0 according to ACD/Percepta™ -14 Software prediction. From the anticorrosion study for carbon steel in 1 mol/L HCl solution done using gravimetric and electrochemical techniques, the following conclusions are drawn:

(1) DMBMI is a promising corrosion inhibitor, which could be used between 25–50 °C.
(2) The anticorrosion performance of DMBMI is concentration dependent. DMBMI concentration in the range of 40–100 mg/L can afford good corrosion inhibition.
(3) DMBMI behaves more as an anodic corrosion inhibitor.
(4) Addition of KI to DMBMI enhanced corrosion inhibition efficiency remarkably through the mechanism of competitive adsorption.
(5) Adsorption energy between the inhibitor and steel surface is high according to Monte Carlo simulations.
(6) Experimental and theoretical results are in conformity.

Conflicts of interest

The authors declare no conflicts of interest.

REFERENCES

[1] Salinas-Solano G, Porcayo-Calderon J, Martinez de la Escalera LM, Cantod J, Casales-Diaz M, Sotelo-Mazon O, et al. Development and evaluation of a green corrosion inhibitor based on rice bran oil obtained from agro-industrial waste. Ind Crops Prod 2018;119:111–24.
[2] Belghiti ME, Echihi S, Mahsoune A, Karzazi Y, Aboulmouhajir A, Dafali A, et al. Piperine derivatives as green corrosion inhibitors on iron surface; DFT, Monte Carlo dynamics study and complexation modes. J Mol Liq 2018;261:62–75.
[3] Moradi M, Song Z, Xiao T. Exopolysaccharide produced by Vibrio neocaledonicus sp. as a green corrosion inhibitor: production and structural characterization. J Mater Sci Technol 2018, http://dx.doi.org/10.1016/j.jmst.2018.05.019.
[4] Taj S, Siddekha A, Papavinasam S, Revie RW. NACE/07, paper No. 07630. Houston, Texas: NACE International Conference & Expo; 2007. p. 1–13.
[5] International Standard for Chemical Safety, Globally Harmonized System of Classification and Labelling of Chemicals (GHS), United Nations Institute for Training and Research Programme Advisory Group.
[6] Singl WP, Bockris JO. Toxicity issues of organic corrosion inhibitors: application of QSAR model. In: Corrosion, paper No. 225. Houston, TX: NACE; 1996.
[7] Tufariello JJ. In: Padwa A, editor. 1,3-dipolar cycloaddition chemistry, vol. 2. New York: Wiley-Interscience; 1984. p. 83.
[8] Berthet M, Cheviet T, Dujardin G, Parrot I, Martinez J. Isoxazolidine: a privileged scaffold for organic and medicinal chemistry. Chem Rev 2016;116:15235–83.
[9] Ali SA, Saeed MT, Rahman SU. The isoxazolidines: a new class of corrosion inhibitors of mild steel in acidic medium. Corros Sci 2003;45:253–66.
[10] Ali SA, El-Shareef AM, Al-Ghamdi RF, Saeed MT. The isoxazolidines: the effects of steric factor and hydrophobic chain length on the corrosion inhibition of mild steel in acidic medium. Corros Sci 2005;47:2659–78.
[11] Yıldırım A, Cetin M. Synthesis and evaluation of new long alkyl side chain acetamide, isoxazolidine and isoxazoline derivatives as corrosion inhibitors. Corros Sci 2008;50:155–65.

[12] Ali SA, Al-Muallem HA, Saeed MT, Rahman SU. Hydrophobic-tailed bicycloisoxazolidines: a comparative study of the newly synthesized compounds on the inhibition of mild steel corrosion in hydrochloric and sulfuric acid media. Corros Sci 2008;50:664–75.
[13] Ali SA, Al-Muallem HA, Rahman SU, Saeed MT. Bis-isoxazolidines: a new class of corrosion inhibitors of mild steel in acidic media,. Corros Sci 2008;50:3070–7.
[14] Ali SA, Mazumder MAJ, Nazal MK, Al-Muallem HA. Assembly of succinic acid and isoxazolidine motifs in a single entity to mitigate CO_2 corrosion of mild steel in saline media. Arab J Chem 2017, http://dx.doi.org/10.1016/j.arabjc.2017.04.005.
[15] Chen P, Zhou H, Liu W, Zhang M, Du Z, Wang X. The synergistic effect of zinc oxide and phenylphosphonic acid zinc salt on the crystallization behavior of poly (lactic acid). Polym Degrad Stab 2015;122:25–35.
[16] Alinejad S, Naderi R, Mahdavian Mohammad. Effect of inhibition synergism of zinc chloride and 2-mercaptobenzoxzole on protective performance of an ecofriendly silane coating on mild steel. J Ind Eng Chem 2017;48:88–98.
[17] Hao Y, Sani LA, Ge T, Fang Q. The synergistic inhibition behaviour of tannic acid and iodide ions on mild steel in H_2SO_4 solutions. Corros Sci 2017;123:158–69.
[18] Feng L, Zhang S, Qiang Y, Xu S, Tan B, Chen S. The synergistic corrosion inhibition study of different chain lengths ionic liquids as green inhibitors for X70 steel in acidic medium. Mater Chem Phys 2018;215:229–41.
[19] Umoren SA, Solomon MM. Synergistic corrosion inhibition effect of metal cations and mixtures of organic compounds: a Review. J Environ Chem Eng 2017;5:246–73.
[20] Umoren SA, Solomon MM. Effect of halide ions on the corrosion inhibition efficiency of different organic species—a review. J Ind Eng Chem 2015;21:81–100.
[21] Murmu M, Saha SKr, Chandra Murmu N, Banerjee P. Effect of stereochemical conformation into the corrosion inhibitive behaviour of double azomethine based Schiff bases on mild steel surface in 1 mol L−1 HCl medium: An experimental, density functional theory and molecular dynamics simulation study. Corros Sci 2019;146:134–51.
[22] Biswas A, Das D, Lgaz H, Pal S, Nair UG. Biopolymer dextrin and poly (vinyl acetate) based graft copolymer as an efficient corrosion inhibitor for mild steel in hydrochloric acid: electrochemical, surface morphological and theoretical studies. J Mol Liq 2019;275:867–78.
[23] Pal S, Lgaz H, Tiwari P, Chung I-M, Ji G, Prakash R. Experimental and theoretical investigation of aqueous and methanolic extracts of *Prunus dulcis* peels as green corrosion inhibitors of mild steel in aggressive chloride media. J Mol Liq 2019;276:347–61.
[24] Saini N, Kumar R, Lgaz H, Salghi R, Chung I-M, Kumar S, et al. Minified dose of urispas drug as better corrosion constraint for soft steel in sulphuric acid solution. J Mol Liq 2018;269:371–80.
[25] Bashir S, Sharma V, Lgaz H, Chung I-M, Singh A, Kumar A. The inhibition action of analgin on the corrosion of mild steel in acidic medium: a combined theoretical and experimental approach. J Mol Liq 2018;263:454–62.
[26] Alhaffar MT, Umoren SA, Obot IB, Ali SA. Isoxazolidine derivatives as corrosion inhibitors for low carbon steel in HCl solution: experimental, theoretical and effect of KI studies. RSC Adv 2018;8:1764–77.
[27] ASTM-G 01–03. ASTM book of standards. West Conshohocken: ASTM; 2003:3.02.
[28] Obot IB, Kaya S, Kay C, Tüzün B. Density Functional Theory (DFT) modeling and Monte Carlo simulation assessment of inhibition performance of some carbohydrazide Schiff bases for steel corrosion. Physica E 2018;80:82–90.
[29] Kumar AM, Babu RS, Obot IB, Gasem Zuhair M. Fabrication of nitrogen doped graphene oxide coatings: experimental and theoretical approach for surface protection. RSC Adv 2015;5:19264–72.
[30] M. El Faydy, R. Touir, M. Ebn Touhami, A. Zarrouk, C. Jama, B. Lakhrissi, L. O. Olasunkanmi, E. E. Ebenso, F. Bentiss. Corrosion inhibition performance of newly synthesized 5-alkoxymethyl-8-hydroxyquinoline derivatives for carbon steel in 1 M HCl solution: experimental, DFT and Monte Carlo simulation studies, Physical Chemistry Chemical Physics, DOI: 10.1039/c8cp03226b.
[31] Obot IB, Kaya S, Kaya C, Tužuň B. Theoretical evaluation of triazine derivatives as steel corrosion inhibitors: DFT and Monte Carlo simulation approaches. Res Chem Intermed 2016;42:4963–83.
[32] Pavithra MK, Venkatesha TV, Vathsals K, Nayana KO. Synergistic effect of halide ions on improving corrosion inhibition behaviour of benzisothiozole-3-piperizine hydrochloride on mild steel in 0.5M H_2SO_4 medium. Corros Sci 2010;52:3811–9.
[33] Brycki BE, Kowalczyk IH, Szulc A, Kaczerewska O, Pakiet M. Organic corrosion inhibitors. In: Aliofkhazraei M, editor. Corrosion inhibitors, principles and recent applications. IntechOpen; 2018., http://dx.doi.org/10.5772/intechopen.72943.
[34] Solomon MM, Umoren SA, Udosoro II, Udoh AP. Inhibitive and adsorption behaviour of carboxymethyl cellulose on mild steel corrosion in sulphuric acid solution. Corros Sci 2010;52:1317–25.
[35] Solomon MM, Gerengi H, Umoren SA. Carboxymethyl cellulose/silver nanoparticles composite: synthesis, characterization and application as a benign corrosion inhibitor for St37 steel in 15% H_2SO_4 medium. ACS Appl Mater Interfaces 2017;9:6376–89.
[36] Farahi A, Bentiss F, Jama C, El Mhammedi MA, Bakasse M. A new approach in modifying ethylene glycol methacrylate phosphate coating formulation by adding sodium montmorillonite to increase corrosion resistance properties. J Alloys Compd 2017;723:1032–8.
[37] Solomon MM, Umoren SA, Obot IB, Sorour AA, Gerengi H. Exploration of dextran for application as corrosion inhibitor for steel in strong acid environment: effect of molecular weight, modification, and temperature on efficiency, ACS Appl. Mater. Interfaces 2018;10:28112–29.
[38] Umoren SA, Solomon MM, Ali SA, Dafalla HDM. Synthesis, characterization, and utilization of a diallylmethylamine-based cyclopolymer for corrosion mitigation in simulated acidizing environment. Mater Sci Eng C 2019;100:897–914.
[39] Roy P, Pal A, Sukul D. Origin of the synergistic effect between polysaccharide and thiourea towards adsorption and corrosion inhibition for mild steel in sulphuric acid. RSC Adv 2014;4:10607–13.
[40] Tao Z, He W, Wang S, Zhang S, Zhou G. A study of differential polarization curves and thermodynamic properties for mild steel in acidic solution with nitrophenyltriazole derivative. Corros Sci 2012;60:205–13.
[41] Hoseinzadeh AR, Danaee I, Maddahy MH, Avei MR. Taurine as a green corrosion inhibitor for AISI 4130 steel alloy in hydrochloric acid solution,. Chemical Engineering Communication 2014;201:380–402.
[42] Solomon MM, Umoren SA. Performance evaluation of poly (methacrylic acid) as corrosion inhibitor in the presence of iodide ions for mild steel in H_2SO_4 solution. J Adhes Sci Technol 2015;29(11):1060–80.
[43] Ramya K, Mohan R, Anupama KK, Joseph A. Electrochemical and theoretical studies on the synergistic interaction and corrosion inhibition of alkyl benzimidazoles and

thiosemicarbazide pair on mild steel in hydrochloric acid. Mater Chem Phys 2015;149–150:632–47.
[44] Mobin M, Khan MA. Adsorption and corrosion inhibition behavior of polyethylene glycol and surfactants additives on mild steel in H_2SO_4. J Mater Eng Perform 2014;23:222–9.
[45] El-Taib Heakal F, Deyab MA, Osman MM, Elkholy AE. Performance of Centaurea cyanus aqueous extract towards corrosion mitigation of carbon steel in saline formation water. Desalination 2018;425:111–22.
[46] Farag AA, Ali TA. The enhancing of 2-pyrazinecarboxamide inhibition effect on the acid corrosion of carbon steel in presence of iodide ions. J Ind Eng Chem 2015;21:627–34.
[47] Vashisht H, Bahadur I, Kumar S, Goyal MS, Kaur G, Singh G, et al. Synergistic interactions between tetra butyl phosphonium hydroxide and iodide ions on the mild steel surface for corrosion inhibition in acidic medium. J Mol Liq 2016;224:19–29.
[48] Hao Y, Sani LA, Ge T, Fang Q. The synergistic inhibition behaviour of tannic acid and iodide ions on mild steel in H_2SO_4 solutions. Corros Sci 2017;123:158–69.
[49] Umoren SA, Solomon MM, Eduok UM, Obot IB, Israel AU. Inhibition of mild steel corrosion in $H2SO_4$ solution by coconut coir dust extract obtained from different solvent systems and synergistic effect of iodide ions: Ethanol and acetone Extracts. J Environ Chem Eng 2014;2:1056.
[50] Gerengi H, Sen N, Uygur I, Solomon MM. Corrosion response of ultra-high strength steels used for automotive applications. Mater Res Express 2019;6:0865a6.
[51] Huang WH, Yen HW, Lee YL. Corrosion behavior and surface analysis of 690MPa-grade offshore steels in chloride media,. J Mater Res Technol 2019;8:1476–85.
[52] Daoud D, Douadi T, Hamani H, Chafaa S, Al-Noaimi M. Corrosion inhibition of mild steel by two new S-heterocyclic compounds in 1 M HCl: experimental and computational study. Corros Sci 2015;94:21–37.
[53] Ghailane T, Balkhmima RA, Ghailane R, Souizi A, Touir R, Ebn Touhami M, et al. Experimental and theoretical studies for mild steel corrosion inhibition in 1 M HCl by two new benzothiazine derivatives. Corros Sci 2013;76:317–24.
[54] Tang YM, Zhang F, Hu SX, Cao ZY, Wu ZL, Jing WH. Novel benzimidazole derivatives as corrosion inhibitors of mild steel in the acidic media. Part I: gravimetric, electrochemical, SEM and XPS studies. Corros Sci 2013;74:271–82.
[55] Zuoa J, Wu B, Luo C, Dong B, Xing F. Preparation of MgAl layered double hydroxides intercalated with nitrite ions and corrosion protection of steel bars in simulated carbonated concrete pore solution. Corros Sci 2019;152:120–9.
[56] Ma X, Jiang X, Xia S, Shan M, Li X, Yu L, et al. New corrosion inhibitor acrylamide methyl ether for mild steel in 1 M HCl. Appl Surf Sci 2016;371:248–57.
[57] Yurt A, Balaban A, Kandemir SU, Bereket G, Erk B. Investigation on someSchiff bases as HCl corrosion inhibitors for carbon steel. Mater Chem Phys 2004;85:420–6.
[58] Pan J, Thierry D, Leygraf C. Electrochemical impedance spectroscopy study of the passive oxide film on titanium for implant application. Electrochim Acta 1996;41:1143–53.
[59] Wang ZB, Hu HX, Zheng YG, Ke W, Qiao YX. Comparison of the corrosion behavior of pure titanium and its alloys in fluoride-containing sulfuric acid. Corros Sci 2016;103:50–65.
[60] Solmaz R, Kardaş G, Çulha M, Yazıcı B, Erbil M. Investigation of adsorption and inhibitive effect of 2-mercaptothiazoline on corrosion of mild steel in hydrochloric acid media. Electrochim Acta 2008;53:5941–52.
[61] Qiang Y, Zhang S, Tan B, Chen S. Evaluation of Ginkgo leaf extract as an eco-friendly corrosion inhibitor of X70 steel in HCl solution. Corros Sci 2018;133:6–16.